Catalysis Today xxx (xxxx) xxx–xxx

Contents lists available at ScienceDirect

Catalysis Today

journal homepage: www.elsevier.com/locate/cattod

Conversion of synthesis gas to aromatics at medium temperature with a fischer tropsch and ZSM-5 dual catalyst bed

J.L. Weber[a], D. Martínez del Monte[b], R. Beerthuis[a], J. Dufour[b,c], C. Martos[b], K.P. de Jong[a], P.E. de Jongh[a,*]

[a] Inorganic Chemistry and Catalysis, Debye Institute for Nanomaterials Science, Utrecht University, the Netherlands
[b] Chemical and Enviromental Engineering Group, Rey Juan Carlos University, Móstoles, Spain
[c] System Analysis Unit, IMDEA Energy, Móstoles, Spain

A B S T R A C T

The production of base chemicals such as olefins and aromatics from synthesis gas is of great interest from both an academic and an industrial point of view. We prepared a bulk iron Fischer Tropsch catalyst promoted with potassium capable of converting synthesis gas to olefins and combined it with an H-ZSM-5 zeolite to convert the formed olefins to aromatics on the zeolite acid sites. All experiments were performed in stacked bed mode to avoid migration of potassium promoters from the iron catalyst to the zeolite, which can deactivate acid sites in the zeolite. Operating at a pressure of 20 bar and temperatures between 250 °C and 300 °C instead of high temperatures of 300 − 350 °C led to a methane selectivity of only 7–14 $\%_C$. Olefins in the range of C_4–C_8 were converted to aromatics in the initial section of the zeolite bed, while further into the zeolite bed C_2-C_3 olefins oligomerized to longer olefins and alkylated light aromatics forming heavier aromatic hydrocarbons. Investigation of the influence of CO conversion on the aromatization of olefins showed a maximum in aromatic selectivity (excluding CO_2) of 18 $\%_C$ at medium CO conversion (X_{CO} = 26–47 %). This work provides detailed insight into the chemical events that occur in bifunctional catalyst beds and can contribute to the development of an industrial process to convert synthesis gas to aromatics in a single reactor.

1. Introduction

To reduce the carbon footprint of chemical processes and the worldwide carbon dioxide emissions, new pathways for the production of chemicals need to be developed [1,2]. The conversion of synthesis gas to chemicals has received significant attention in the past years, since it opens a route for the production of platform chemicals for the chemical industry that is independent of crude oil. Synthesis gas is a mixture of carbon monoxide and hydrogen and can be derived from carbon containing sources such as shale gas, natural gas, coal, biomass, or from CO_2 with renewable hydrogen [3–6].

Recent publications have mostly focused on the synthesis of short olefins (C_2-C_4) [7–12]. Synthesis gas can be converted directly using the Fischer-Tropsch to olefins (FTO) process, which allows to form C_2-C_4 olefins with 65 $\%_C$ selectivity within the hydrocarbons (excluding CO_2) [7,8]. Typically, the product distribution of the Fischer-Tropsch synthesis is described with the Anderson-Schulz-Flory (ASF) distribution, which means that the preferential formation of short olefins implies an undesirably high methane fraction [13]. The presence of sodium and sulfur promoters in iron (carbide) based FTO catalysts, however, can lead to a deviation from the Anderson-Schulz-Flory distribution with less methane and an increased olefin to paraffin ratio [14–16].

Alternatively, a bifunctional catalyst system can be used to convert synthesis gas in a single reactor to reactive oxygenate intermediates such as methanol [17], dimethyl ether [18], or ketene [10,19] on a metal oxide catalyst and subsequently to short olefins using solid acids such as zeolites. The product distribution of these bifunctional catalyst systems is determined by the pore confinement of the zeolite and can be controlled by the pore structure and acid strength. Using a SAPO-34 zeolite with 8-membered rings led to the formation of a mixture of C_2-C_4 olefins with a total selectivity of 80 $\%_C$ [10,20], whereas a zeolite with mordenite structure and selectively blocked 12-membered ring sites formed ethylene in the 8-membered ring side pockets with 73 $\%_C$ selectivity [19]. Larger pore diameters of the H-ZSM-5 zeolite consisting of a 10-membered ring pore system allowed the formation of aromatic hydrocarbons from oxygenate intermediates with selectivities as high as 80 $\%_C$ [17,21–23].

To convert synthesis gas into aromatics via olefinic intermediates instead of oxygenates, an iron (carbide) based Fischer-Tropsch catalyst [24] can be combined with an H-ZSM-5 zeolite [25–31]. Combining a sodium and sulfur promoted iron (carbide) FTO catalyst with the acid properties of a H-ZSM-5 zeolite in a high temperature and low pressure process (400 °C, 1 bar) resulted in the formation of C_6-C_8 aromatics with

* Corresponding author.
E-mail address: P.E.deJongh@uu.nl (P.E. de Jongh).

https://doi.org/10.1016/j.cattod.2020.05.016
Received 22 November 2019; Received in revised form 8 April 2020; Accepted 5 May 2020

reasonable selectivity of up to 27 $\%_C$, while C_2-C_4 olefins are preserved with 41 $\%_C$ selectivity [32]. We found that the pathway for aromatization of olefins in this high temperature process followed dehydro-aromatization rather than hydrogen transfer, resulting in a C_2-C_4 paraffin selectivity of only 4–10 $\%_C$ and decreased hydrogen to carbon ratio in the overall hydrocarbon products compared to the FTO catalyst without zeolite. Furthermore, the activity of the FTO function was enhanced by close proximity of the zeolite, due to enhanced formation of iron carbides.

However, the close proximity also led to the migration of sodium ions from the FTO catalyst to the acid sites of the zeolite, resulting in decreased acidity of the zeolite and loss of promotion effect of the sodium and sulfur and therefore increased methane selectivity [33,34]. This migration of sodium ions can be mitigated by increasing the distance between the FTO catalyst and the zeolite for instance by operating in stacked bed mode with the zeolite downstream of the FTO catalyst [35–37].

Typically, the low temperature Fischer-Tropsch (LT-FT) process is operated at temperatures between 200 °C and 240 °C and pressures of 25 – 45 bar, whereas the high temperature Fischer-Tropsch (HT-FT) process takes place between 300 °C and 350 °C and 20 – 40 bar [38]. In previous publications [32,33], we discussed fundamental insights for reaction conditions (400 °C and 1 bar) that are not applied in industrial processes. These harsh conditions caused rapid deactivation of the bifunctional catalysts.

In this work, we discuss a bulk iron catalyst promoted with potassium to convert synthesis gas to olefins at 250 – 300 °C and 20 bar, avoiding rapid deactivation and also shifting the Anderson-Schulz-Flory distribution to higher alpha values by operating at relatively low temperatures. This results in an increase of average chain length of the hydrocarbon products. Furthermore, placing an H-ZSM-5 zeolite downstream of the iron catalyst in a stacked bed mode allows to convert the olefins formed on the iron catalyst into aromatics in a single reactor.

We focused in this work on the influence of the chain length of olefin intermediates on the aromatization, and show that long olefins are converted in the initial section of the zeolite bed followed by oligomerization of short olefins and further aromatization in the consecutive sections of the zeolite bed. The yield of aromatics decreases with increasing CO conversion.

2. Experimental section

2.1. Catalyst preparation

We prepared iron oxide by precipitation from an iron nitrate nonahydrate solution followed by decomposition of the precursor. 20.32 g $Fe(NO_3)_3$ 9 H_2O (Acros Organics, for analysis 99 + %) was dissolved in 500 mL demineralized water (0.1 mol/L, initial pH 1.67). The pH was increased to 10 by adding an ammonia solution (Merck, 28 – 30 wt-%) under vigorous stirring at 25 °C within 10 s to 20 s. One hour after pH 10 was reached, the stirring was turned off and the precipitate was let to sediment for 16 h at 25 °C. After sedimentation, the supernatant was decanted and the precipitate was centrifuged at 3000 rpm for 5 min. Afterwards the remaining supernatant was decanted and the precipitate was re-dispersed in 300 mL demineralized water, centrifuged for 10 min at 3000 rpm and the supernatant was decanted. This washing step was performed in total three times. The resulting gel was dried in an oven in static air at 120 °C for 16 h and afterwards transferred into a quartz fixed bed reactor tube with ~20 mm inner diameter and heated with 5 °C/min to 350 °C (2 h hold time) in a flow of 100 mL/min nitrogen. The resulting material showed a yield of 3.48 g (87 % of the theoretical yield) with a total pore volume of 0.25 mL/g and was denoted as "Fe".

The potassium promoter was introduced by incipient wetness impregnation of 3.48 g of the calcined iron oxide powder (Fe) with a solution containing potassium nitrate (Sigma Aldrich, ReagentPlus > 99 %, 217.0 mg/mL in demineralized water, 2.15 mol/L, 0.25 mL solution per gram of Fe), resulting in 1.95 wt-% K/Fe_2O_3 and a molar ratio of K:Fe = 0.043 at/at. After impregnation the material was dried and heated with 5 °C/min to 120 °C under 100 mL/min nitrogen flow, where it was held for 2 h and subsequently heated to 350 °C with 5 °C/min (1 h hold time) in a quartz fixed bed reactor tube with ~20 mm inner diameter. The heat-treated sample was pelletized (4 t with a 20 mm piston), ground in a mortar and sieved to a sieve fraction between 150 – 212 µm. The resulting potassium-promoted iron catalyst was denoted as "FeK".

To convert the ZSM-5 zeolite (Zeolyst, Si:Al = 15 at/at) from the ammonium form to the proton form, calcination was carried out at 550 °C (4.4 °C/min) for 4 h in a muffle stove in static air. Afterwards, the calcined zeolite was pelletized (4 t with a 20 mm piston), ground in a mortar and sieved to a sieve fraction of 150 – 212 µm.

2.2. Catalyst characterization

Thermogravimetric analysis (TGA) in nitrogen flow of the dried precipitate before calcination was performed on a TA Instruments Q50 thermal gravimetric analyzer to determine the optimum temperature for calcination. An amount of 20 – 25 mg sample was loaded in a platinum pan and heated under 60 mL/min nitrogen flow with 15 °C/min to 600 °C. The carbon deposition of the spent catalysts was analyzed with a Perkin Elmer TGA 8000 with autosampler. Here, 5 – 10 mg spent catalyst were weighed in ceramic plans and heated with 15 °C/min to 700 °C under 60 mL/min synthetic air (20 vol-% O_2 and 80 vol-% N_2) flow.

To gain information about the crystal phase and crystal size of the dried and calcined precipitate, X-ray diffractograms (XRD) were recorded on a Bruker D2 Phaser, equipped with a Co source operating at λ = 1.789 Å between 2Θ = 10-80° with an increment of 0.07° per step and 1 s exposure time.

N_2-physisorption at −196 °C was carried out on a Micromeritics TriStar 3000 to determine the specific surface area and mesopore volume of the calcined and promoted bulk iron catalyst before and after the catalytic testing. The fresh and spent zeolite catalysts were analyzed using Ar-physisorption at −196 °C. Prior to measurement, the materials were dried in nitrogen flow at 250 °C for 16 h. The total pore volume was determined from single point adsorption at p/p_0 = 0.995. The isotherms of the promoted and calcined iron catalyst can be found in the supporting information, Fig. S1.

Inductively coupled plasma optical emission spectroscopy (ICP-OES) was carried out on a Spectro Arcos after digestion of the promoted and calcined bulk iron catalyst in *aqua regia*.

Bright-field transmission electron microscopy and scanning transmission electron microscopy in combination with energy dispersive X-ray spectroscopy (STEM-EDX) in high annular angle dark field mode (HAADF) were performed using a FEI Talos F200X, equipped with a high brightness field emission gun and a Super-X G2 EDX detector and operating at 200 kV. The samples were prepared by dispersing in methanol and ultra-sonification for ~5 min. Afterwards, a drop of the sample dispersed in methanol was placed onto a carbon TEM grid and let dry. Scanning electron microscopy was performed on a Helios NanoLab G3 in immersion mode and using 5 kV acceleration. The samples were prepared by sprinkling a finely crushed powder onto adhesive SEM sample holders.

2.3. Catalytic performance

To investigate the performance of the promoted bulk iron catalyst in combination with the H-ZSM-5 zeolite in the conversion of synthesis gas to olefins and aromatics, experiments were carried out in a 16-channel parallel reactor setup (Avantium Flowrence). The calcined and sieved catalysts were loaded into stainless steel reactor tubes with 2.6 mm inner diameter in a stacked bed configuration with the zeolite downstream of the iron. The iron catalyst had beforehand been diluted

with a 5-fold mass of silicon carbide (Alfa Aesar, > 98 %, 46 grit) to avoid clogging and channeling in the iron catalyst bed. An illustration of insufficient dilution of the iron catalyst with silicon carbide can be found in the supporting information (Fig. S2). Prior to use, the silicon carbide was calcined in a muffle stove in static air at 550 °C (4.4 °C/min) for 5 h to remove potential contaminants and sieved to a fraction between 212 µm and 425 µm.

To study the influence of zeolite bed height on the aromatization, between 5 mg and 40 mg H-ZSM-5 was loaded into the reactors, resulting in zeolite bed heights of 2–17 mm. After placing a ~1 mm layer of silicon carbide on top of the zeolite bed, the iron catalyst was loaded into the reactor. To operate at similar CO conversion levels and therefore achieve a better comparison of the resulting selectivities, more catalyst was loaded into the reactor when operating at lower reaction temperatures. For the experiments at 250 °C, 40 mg iron catalyst was loaded. At 275 °C and 300 °C the amount was reduced to 20 mg and 10 mg, respectively. The flow rate of synthesis gas was the same for all reactors but as the amount of catalyst differed per reactor, the corresponding gas hourly space velocities (GHSV, volume flow of feed gas divided by FeK catalyst bed volume) varied and were 10,000 h^{-1}at 250 °C, 20,000 h^{-1}at 275 °C and 40,000 h^{-1}at 300 °C.

Furthermore, experiments were conducted to investigate the influence of CO conversion on the aromatization, using a zeolite bed with fixed height. 20 mg of H-ZSM-5 was loaded into the bottom of the reactor, giving a zeolite bed height of 9 mm. After placing a ~1 mm silicon carbide layer on top of the zeolite bed, 5–50 mg of iron catalyst were loaded into the reactor.

After the reactors were placed in the test unit, the iron catalysts were reduced *in-situ* by heating to 350 °C with 5 °C/min in 6.25 mL_{STP}/min 30 % H_2 in N_2 v/v at 1 bar pressure and holding these conditions for 2 h. Afterwards, the reactors were cooled down to reaction temperature between 250–300 °C with 5 °C/min. After switching to synthesis gas with 7.5 mL_{STP}/min and CO:H_2:He = 9:9:1 v/v/v, the pressure in the reactors was increased to 20 bar. The gas flowing through the reactors was diluted with 25 mL_{STD}/min N_2 at the end of every individual reactor in the high-pressure section to avoid product condensation. Synthesis gas and the N_2-diluent were distributed over the reactors with individual sets of capillaries, creating a pressure-drop of 15–20 bar and avoiding reverse flow through the reactors. The gases and C_1-C_{17} hydrocarbon products were analyzed with an online gas-chromatograph Agilent 7890-B, equipped with two flame ionization detectors and a thermal conductivity detector. The iron (-carbide based catalysts showed high water-gas-shift activity ($CO + H_2O \leftrightarrow CO_2 + H_2$), resulting in CO_2 selectivity of ~50 $\%_C$. Reported product selectivities are given as hydrocarbon distribution excluding CO_2.

After the reaction finished, the hydrocarbon products were stripped from the catalysts by flowing 50 % H_2 in N_2 v/v with 12.5 mL_{STP}/min at 350 °C and 10 bar for 4 h, followed by stripping at 300 °C and 1 bar for 5 h with the same flow conditions. The spent catalysts were characterized after hydrogen stripping.

3. Results and discussion

3.1. Characterization

To determine an appropriate temperature for heat treatment, the weight loss of the dried precipitate was measured while heating in nitrogen flow. The weight loss roughly between 200 °C and 400 °C (Fig. 1) of about 8 wt% corresponds to that expected from the dehydration of FeOOH to Fe_2O_3. The conversion of FeOOH to Fe_2O_3 was complete at 350 °C, which was hence chosen as the decomposition temperature to convert the dried precipitate into the "Fe" material.

XRD (Fig. 2) of the precipitate after drying at 120 °C in air showed the presence of crystalline goethite (α-FeOOH) and hematite (α-Fe_2O_3). After further heat treatment at 350 °C in a nitrogen flow only crystalline hematite was observed, showing that temperature of 350 °C for the heat

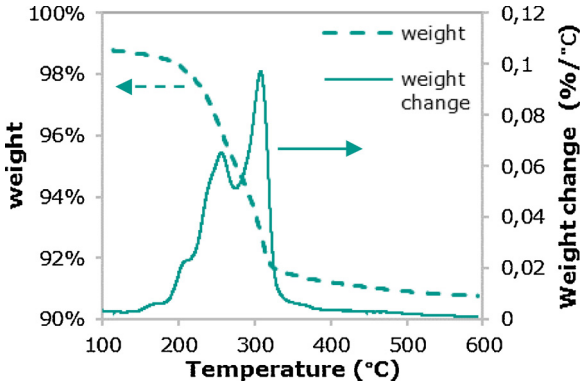

Fig. 1. Normalized weight and weight change during thermogravimetric analysis in nitrogen flow as function of temperature of the iron precipitate after drying. Heating rate: 15 °C/min.

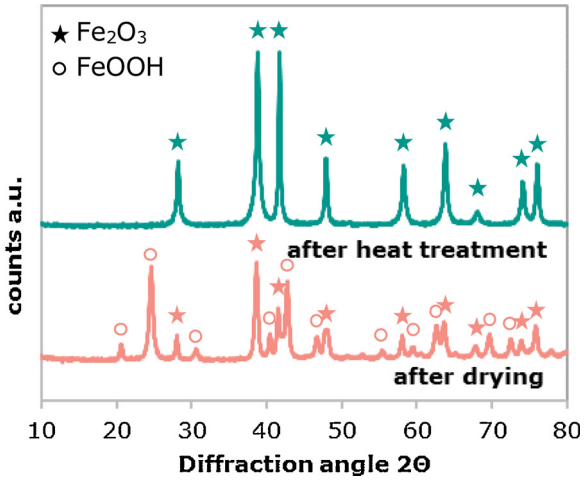

Fig. 2. X-ray diffractogram of the precipitate after drying and after subsequent heat treatment at 350 °C in nitrogen flow for 2 h. Stars: XRD pattern of Fe_2O_3, circles: FeOOH.

treatment was sufficient to convert the dried precipitate into iron oxide ("Fe" material).

A transmission electron micrograph and scanning electron micrograph of the iron-potassium catalyst (FeK) after heat treatment (120 °C for 2 h followed by 350 °C for 1 h in nitrogen flow) can be found in Fig. 3. The sample exhibited a needle-like structure. This is as expected as goethite (α-FeOOH) is known to form a needle-like structure when formed via precipitation from an iron nitrate solution [39]. This structure seemed to be maintained during the heat treatment at 350 °C in nitrogen flow. ICP-OES showed an iron content of 65.4 wt% and 1.95 wt% potassium in the promoted and calcined iron catalyst. This resulted in a ratio of K:Fe = 0.043 at/at, which is in good agreement with the values we expected (nominal composition: 68.0 wt.-% Fe, 1.95 wt.-% K, balance oxygen).

3.2. Catalytic performance

In this section, we discuss the performance of the iron catalysts at temperatures between 250–300 °C and 20 bar pressure in terms of activity and selectivity of the iron catalyst with and without zeolite present. Also, we investigated the influence of the zeolite bed height, and hence the residence time of olefins formed on the iron catalyst in the zeolite bed, in stacked bed. Placing various amounts of zeolite downstream of the iron catalyst allowed us to follow aromatization at different positions in the zeolite bed. Finally, the influence of CO conversion on the aromatization in a zeolite bed with fixed height is

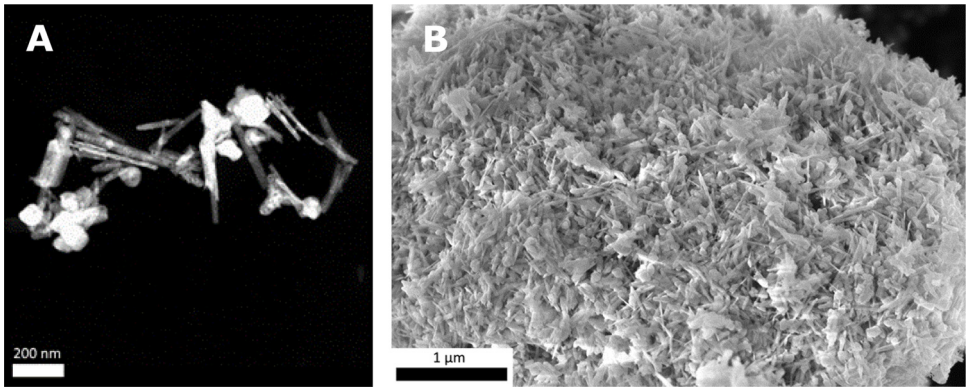

Fig. 3. A: High annular angle dark field scanning transmission electron microscopy (HAADF-STEM) image of FeK after heat treatment and **B:** scanning electron microscopy image of FeK after heat treatment.

discussed.

3.2.1. Influence of reaction temperature on the performance of the iron catalyst

The experiments to evaluate the performance of the potassium promoted iron catalyst were conducted with CO conversions of 15–20 %, allowing a direct comparison of the selectivities at similar conversion. This was achieved by decreasing the amount of iron catalyst placed inside the reactor with increasing reaction temperature, while keeping the flow constant for all experiments.

At 250 °C and a GHSV of 10,000 h^{-1}, FeK showed a CO conversion of 17 % in the initial phase of the reaction. However, the CO conversion decreased upon the first 15 h on stream and stabilized at 6–7 % after − 20 h (Fig. 4-A). Increasing the reaction temperature to 275 °C and the GHSV to 20,000 h^{-1}, led to a CO conversion between 13 % and 16 %. The experiment conducted at a reaction temperature of 300 °C and GHSV of 40,000 h^{-1} showed 19 % CO conversion in the initial phase of the reaction, gradually decreasing to 13 % conversion.

The activity normalized to the mass of iron (iron time yield, FTY, mind that different amounts of iron were loaded for the different experiments to achieve similar initial conversion) decreased from 0.8×10^{-5} mol CO g_{Fe}^{-1} s^{-1} to 0.3×10^{-5} mol CO g_{Fe}^{-1} s^{-1} for the experiments performed at 250 °C (Fig. 4-B). At 275 °C the FTY was higher, 1.2–1.4 $\times 10^{-5}$ mol CO g_{Fe}^{-1} s^{-1}, due to the increased reaction temperature. The FTY decreased from 3.4×10^{-5} mol CO g_{Fe}^{-1} s^{-1} to 2.3×10^{-5} mol CO g_{Fe}^{-1} s^{-1} within the first 40 h on stream, when operated at 300 °C.

In general, the iron mass normalized activity increased with increasing reaction temperature, as expected. The deactivation was more severe at 250 °C than at 275 − 300 °C. We ascribe this decrease in activity to hydrocarbon deposition on the surface of the catalyst [40,41]. These hydrocarbons are less likely to be removed at low operating temperatures.

FeK produced 8 % methane at 250 °C, whereas the selectivity to methane increased to 14 $\%_C$ at 275 °C and 300 °C (Fig. 5). These methane selectivities are similar to the selectivities achieved with a supported FTO catalyst promoted with sodium and sulfur and operated at high temperature and low pressure of usually 340 − 350 °C [32].

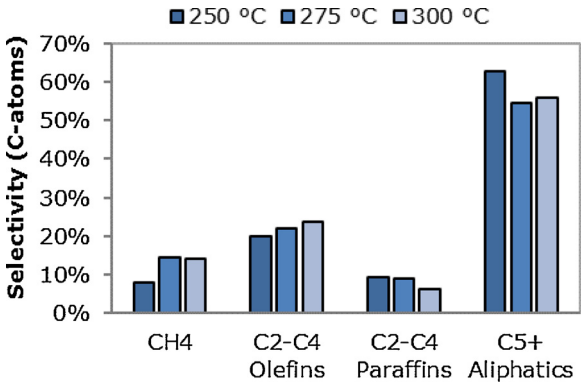

Fig. 5. Hydrocarbon product distribution based on carbon atom selectivity (CO_2 free) of FeK tested at 250 °C, 275 °C and 300 °C and CO conversion between 15–20 %. Reaction conditions: 250 − 300 °C, 20 bar, CO:H_2 = 1 v/v. FeK was tested at 250 °C with FeK based GHSV of 10,000 h^{-1}, at 275 °C with GHSV of 20,000 h^{-1} and 300 °C with GHSV of 40,000 h^{-1} to reach same conversion levels in the initial phase of the reaction (TOS = 6-12 h) of 15–20 %. The corresponding product formation rates can be found in the supporting information, Figure S6-C.

The C_2-C_4 fraction (sum of olefins and paraffins) in the hydrocarbon products was 29–31 $\%_C$, independent of the temperature. However, the contribution of olefins to the C_2-C_4 fraction increased with reaction temperature from 69 $\%_C$ at 250 °C and 71 $\%_C$ at 275 °C to 80 $\%_C$ at 300 °C [42]. This shows that chain termination via *β*-hydride abstraction is enhanced with increasing reaction temperature, and/or *α*-hydrogenation is reduced (Fig. S3, supporting information). The selectivity to aliphatic C_{5+} products decreased from 63 $\%_C$ at 250 °C to 54

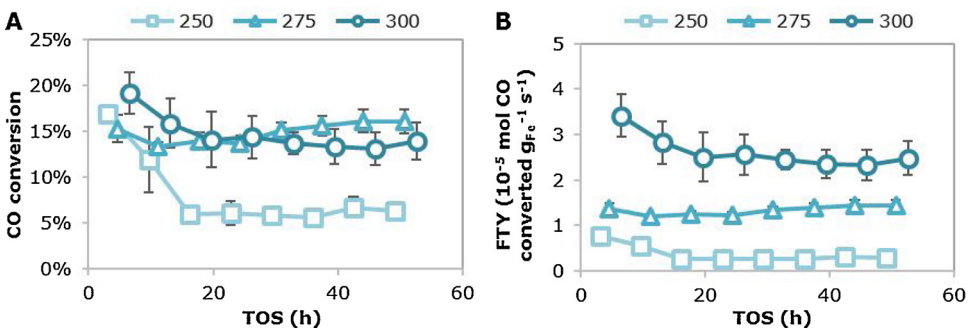

Fig. 4. Activity of FeK as function of time at 250 °C, 275 °C and 300 °C. **A:** CO conversion as function of time on stream. **B:** FTY (iron time yield, moles of CO converted per gram of iron and second) as function of time on stream. Reaction conditions: 250 − 300 °C, 20 bar, CO:H_2 = 1 v/v. FeK was tested at 250 °C with an FeK based GHSV of 10,000 h^{-1}, at 275 °C with GHSV of 20,000 h^{-1} and 300 °C with GHSV of 40,000 h^{-1} to reach same conversion levels (15–20 %) in the initial phase of the reaction (TOS = 6 − 12 h). Error bars indicate standard deviation from four experiments at 250 − 275 °C and seven experiments at 300 °C.

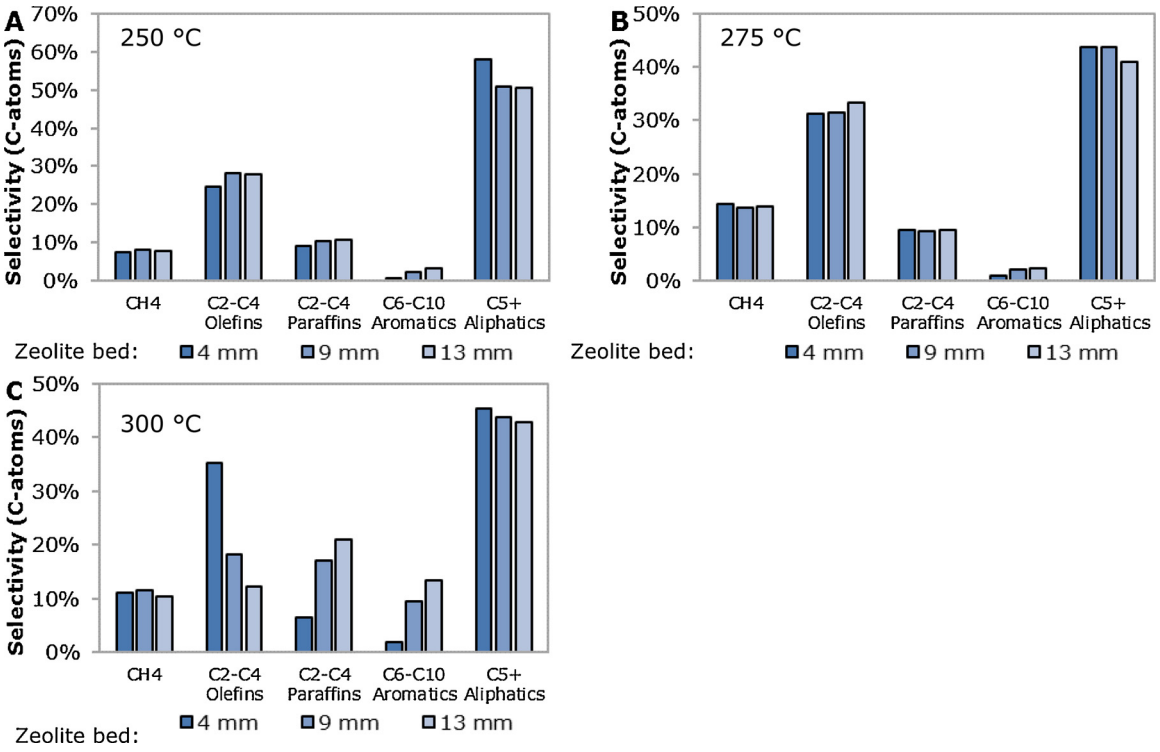

Fig. 6. Hydrocarbon distribution based on carbon atom selectivity (CO_2 free) of FeK and H-ZSM-5 in stacked bed mode with zeolite bed height between 4 mm and 13 mm tested at **A:** 250 °C, **B:** 275 °C and **C:** 300 °C and CO conversion between 15–20 %. Reaction conditions: 250 − 300 °C, 20 bar, CO:H_2 = 1 v/v. FeK was tested at 250 °C with FeK based GHSV of 10,000 h^{-1}, at 275 °C with GHSV of 20,000 h^{-1} and 300 °C with GHSV of 40,000 h^{-1} to reach same conversion levels in the initial phase of the reaction (TOS = 6 − 12 h) of 15–20 %. The corresponding product formation rates can be found in the supporting information, Figure S6-D to Figure S6-F.

$\%_C$ and 56 $\%_C$ at 275 °C and 300 °C, respectively.

These relatively low methane selectivities as well as the high C_{5+} selectivities correspond to α-values between 0.70 and 0.75 for the ASF distribution for all temperatures tested. An α-value in this range can be beneficial for the aromatization of olefin intermediates, because this gives the highest selectivity to the C_6-C_{10} fraction according to the ASF distribution (Fig. S4, supporting information) for which no oligomerization is needed to form C_6-C_{10} aromatics. Additionally, the olefin/paraffin ratio of the products increased with reaction temperature, resulting in higher selectivity to reactive olefinic intermediates at higher temperatures.

3.2.2. *Influence of zeolite bed height on aromatization*

To convert the olefins formed on the iron catalyst to aromatics, H-ZSM-5 zeolite beds with different heights were placed downstream of the FeK bed in stacked mode. Fig. 6 A–C shows an overview of the resulting selectivities, obtained at temperatures between 250 − 300 °C. Indeed the selectivity to methane did not change significantly upon the addition of H-ZSM-5 zeolite downstream of FeK, confirming that the potassium promoter did not migrate from the iron catalyst to the zeolite resulting in catalyst deactivation, as reported earlier [33].

The selectivity to C_2-C_4 olefins increased upon placing a zeolite bed downstream of FeK at 250 °C and 275 °C from 20 $\%_C$ to 28 $\%_C$ and 22 $\%_C$ to 33 $\%_C$, respectively (Fig. 6-A and B). Simultaneously, the selectivity to C_{5+} aliphatics decreased in these experiments from 63 $\%_C$ to 50 $\%_C$ and from 54 $\%_C$ to 41 $\%_C$, suggesting that the increase in C_2-C_4 olefins was caused by partial cracking of the C_{5+} fraction. C_2-C_4 paraffins were not affected and remained between 9 $\%_C$ and 11 $\%_C$ for the experiments conducted at 250 °C and 275 °C. Furthermore, C_6-C_{10} aromatics were formed with only 2–3 $\%_C$ selectivity at these temperatures.

Results at 300 °C were markedly different (Fig. 6-C). With a zeolite bed of 4 mm the selectivity to C_2-C_4 olefins increased from 24 $\%_C$ to 35 $\%_C$, whereas the C_{5+} selectivity decreased from 56 $\%_C$ to 43 $\%_C$ and C_6-C_{10} aromatics were formed with 2 $\%_C$ selectivity. With increasing zeolite bed height to 13 mm, the selectivity to C_2-C_4 olefins decreased to 12 $\%_C$, whereas C_2-C_4 paraffins increased from 6 $\%_C$ to 21 $\%_C$ and C_6-C_{10} aromatics increased to 13 $\%_C$.

The simultaneous decrease in C_2-C_4 olefin selectivity and increase in C_2-C_4 paraffin and C_6-C_{10} aromatic selectivity indicates that the aromatization of olefins followed hydrogen transfer. Here, hydrogen is transferred from olefins molecules to other olefin molecules forming paraffins and dienes, after which the dienes undergo cyclization and aromatization [43,44]. As at 300 °C C_6-C_{10} aromatics were formed with up to 13 $\%_C$ selectivity with a 13 mm zeolite bed, we will discuss the aromatization at 300 °C more in detail in the following section.

The selectivities to C_2-C_3 olefins, C_4-C_8 olefins and C_6-C_{10} aromatics as function of zeolite bed height at 300 °C are shown in Fig. 7-A. The iron catalyst showed at 300 °C a selectivity to C_2-C_3 olefins of 23 $\%_C$ and C_4-C_8 olefins of 32 $\%_C$, whereas no aromatics were formed under these conditions. Placing H-ZSM-5 zeolite downstream of FeK with a bed height of 2 − 4 mm did not change the selectivity to C_2-C_3 olefins, but led to a sharp decrease of in C_4-C_8 olefins of 19 $\%_C$ with a zeolite bed of 2 mm. At the same time C_6-C_{10} aromatics were formed with low selectivity of 2–3 $\%_C$ at zeolite bed heights of 2 − 4 mm.

Higher zeolite beds led to a gradual decrease of the C_2-C_3 olefin selectivity from 10 $\%_C$ at 7 mm zeolite bed height to 2 $\%_C$ at 17 mm, whereas the selectivity of C_4-C_8 olefins increased to 23–24 $\%_C$. at 7 mm, followed by a gradual decrease to 4 $\%_C$ C_4-C_8 olefins at a zeolite bed height of 17 mm. With increasing amount of zeolite downstream of FeK the selectivity to C_6-C_{10} aromatics increased gradually to 18 $\%_C$ at 17 mm zeolite bed height.

In the initial section of the zeolite bed, C_4-C_8 olefins were exclusively converted to aromatics with low selectivity, whereas the C_2-C_3 olefins remained untouched. In the further course of the zeolite bed (4 mm–7 mm), C_2-C_3 olefins underwent oligomerization forming C_4-C_8

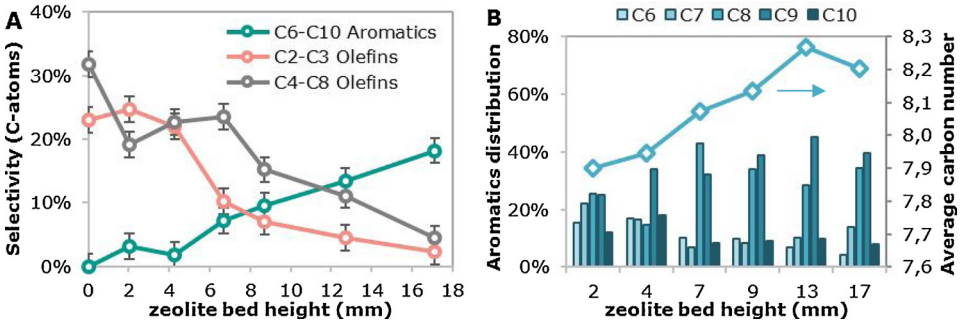

Fig. 7. A: Selectivity of C_2-C_3 olefins, C_4-C_8 olefins and C_6-C_{10} aromatics as function of zeolite bed height for stacked bed experiments with FeK and H-ZSM-5 zeolite at 300 °C, and **B:** Mol fraction (in %) of the different C_6-C_{10} aromatics within the total aromatics production (columns) and average carbon number of the aromatics (diamonds) as function zeolite bed height for stacked bed experiments with FeK and H-ZSM-5 zeolite at 300 °C. Reaction conditions: 300 °C, 20 bar, CO:H_2 = 1 v/v, GHSV of 40,000 h^{-1}, TOS = 6 – 9 h, CO conversion of 15–20 %. The volume of the zeolite bed was varied to achieve zeolite based GHSV between 4500 h^{-1} and 40,000 h^{-1}. The corresponding graphs for 250 °C and 275 °C can be found in Fig. S6.

olefins. These C_4-C_8 olefins were consecutively converted into aromatics.

Fig. 7-B shows the distribution and the average carbon number within the C_6-C_{10} aromatics fraction as function of zeolite bed height. With increasing height of the zeolite bed the average carbon number of the C_6-C_{10} aromatics increased from 7.9 at 2 mm zeolite bed height to 8.3 at 13 mm. Furthermore, ethylmethylbenzene was identified as main aromatic product for a zeolite bed height of 7 mm and higher (a detailed distribution of the aromatic products can be found in the supporting information, Fig. S5). Therefore, we hypothesize that the C_2-C_3 olefins and especially ethylene not only contribute to the oligomerization to form longer olefins, but also in the alkylation of light aromatics, forming heavier aromatic products.

It is clear that longer olefins in the range of C_3-C_8 are converted to aromatics already in the initial section of the zeolite bed, whereas short olefins (C_2-C_3) undergo oligomerization and alkylation of aromatics in the consecutive section of the zeolite bed. Further details of the influence of the zeolite bed height on the cracking and isomerization behavior can be found in the supporting information (Fig. S7-S8).

3.2.3. Influence of CO conversion on aromatization

To investigate the influence of CO conversion on the aromatization through an H-ZSM-5 zeolite bed, the amount of FeK upstream of the zeolite bed was varied to achieve FeK based GHSV between 8000 h^{-1} and 75,000 h^{-1}, whereas the height of the zeolite bed was kept at 9 mm.

Operating at a low GHSV of 8000 h^{-1} at a temperature of 300 °C in 20 bar synthesis gas (CO:H_2 = 1 v/v) resulted in a high CO conversion (71 %) while by increasing the GHSV, the CO conversion was reduced to 3.5 % at a GHSV of 75,000 h^{-1} (Fig. 8-A). The selectivity to C_6-C_{10} aromatics was 2.1 $\%_C$ at 71 % CO conversion and gradually increased to 3.0 $\%_C$ at 41 % CO conversion. Operating at a medium GHSV of 37,000 h^{-1} led to a drastic increase in C_6-C_{10} aromatics selectivity to 10 $\%_C$ with 29 % CO conversion.

At low CO conversion of 3.5 % a very low yield of 0.1 $\%_C$ to C_6-C_{10} aromatics was observed, whereas, with increasing CO conversion to 26–47 % also the yield to C_6-C_{10} aromatics increased to 2.8–3.2 $\%_C$ (Fig. 8-B). However, the yield decreased to 1.9–2.0 $\%_C$ at high CO conversion between 53 % and 76 %. From this we conclude that the yield to aromatics is limited by the low CO conversion when operating at too high space velocities, while at too low GHSV the CO conversion increased but at the expense of selectivity loss. This also resulted in lowered yield to C_6-C_{10} aromatics. With higher conversions more olefins were fed into the zeolite bed, whereas the zeolite bed height and hence the amount of available active acid sites remained constant. As a result, more olefins were fed into the zeolite than could be converted. At medium CO conversion the optimum balance between selectivity and CO conversion led to a maximum yield to C6-C10 aromatics, showing that the composition of a stacked catalyst bed is a key parameter in bifunctional catalysis and required expanded attention.

3.3. Spent catalyst analysis

The pore volume as well as the specific surface area of the fresh FeK was measured using nitrogen physisorption and can be found in Table 1 next to argon physisorption data obtained for the fresh and spent H-ZSM-5 zeolite.

Fresh FeK showed a specific surface area of 32 m^2/g and 0.23 mL/g pore volume with mostly mesopores. The surface area and pore volume of the spent FeK were too low to be determined by physisorption. The fresh H-ZSM-5 zeolite had a specific surface area of 430 m^2/g and 0.22 mL/g pore volume, mostly micropores. The spent zeolite (after 50 h, 300 °C, 20 bar, CO:H_2 = 1 v/v, FeK based GHSV of 40,000 h^{-1} and zeolite bed height of 9 mm) showed a specific surface area of 260 m^2/g and reduced pore volume of 0.11 mL/g. The decrease in pore volume was mostly caused by the decrease in micropore volume. Porosity analysis of the spent FeK was not possible, due to hydrocarbon products being present on the surface of the catalyst. The decrease in specific surface area and pore volume of the spent zeolite was assigned to coke formation inside the micropores upon aromatization of olefins.

Fig. 9 shows EM images of FeK after reduction and after 50 h on stream. The initial needle structure was partially maintained upon

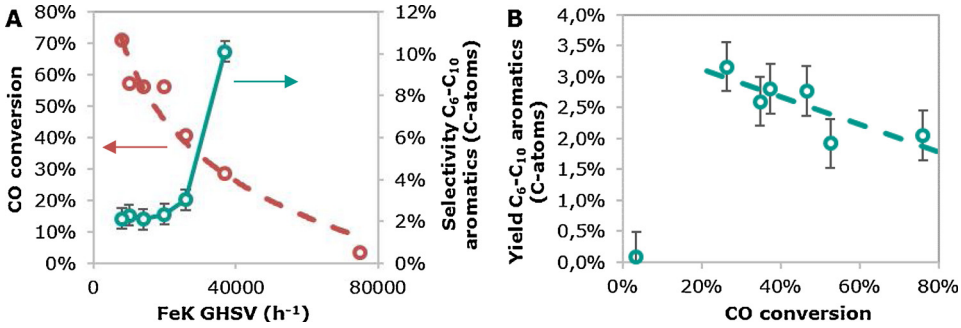

Fig. 8. A: CO conversion and selectivity to C_6-C_{10} aromatics (CO_2 free) as function of FeK based GHSV and **B:** Yield to C_6-C_{10} aromatics as function of CO conversion for stacked bed experiments of FeK and zeolite operated at 300 °C. Reaction conditions: 300 °C, 20 bar, CO:H_2 = 1 v/v, FeK based GHSV 8000-75,000 h^{-1} and zeolite bed height of 9 mm, TOS = 3 – 5 h. Selectivities were not reported for CO conversions below 5 %, as the signal to noise ratio became too small.

Table 1
Surface area and pore volume of fresh FeK determined with nitrogen physisorption and fresh and spent H-ZSM-5 determined with argon physisorption.

Sample	Surface area	V_{total}	V_{micro}	V_{meso}
	m^2/g	mL/g	mL/g	mL/g
FeK	32	0.23	0.005	0.22
H-ZSM-5	430	0.22	0.15	0.07
spent H-ZSM-5[a]	260	0.11	0.05	0.05

[a] reaction conditions: 300 °C, 20 bar, CO:H2 = 1 v/v, FeK based GHSV of 40,000 h-1, zeolite bed height of 9 mm, after 50 h.

reduction at 350 °C for 2 h in 30 % H_2 in N_2 (v/v) at 1 bar. After applying Fischer-Tropsch conditions of 300 °C, 20 bar and CO:H_2 = 1 v/v, the iron catalyst showed fragmentation of the needles (Fig. 9-B and D, TEM and SEM images for spent catalysts operated at 250 °C and 275 °C can be found in the supporting information, Fig. S9). In bright-field TEM and SEM, we also found that the spent iron catalyst was embedded in hydrocarbon products. This is in agreement with the observation of the activity decreasing in the first 10 h of the experiments. In the initial phase of the reaction a product layer is formed around the iron (-carbide) based catalysts. This layer hindered the diffusion of synthesis gas to the active sites of the iron (-carbide) based catalyst.

The thermogravimetric analysis of the spent catalysts showed that the amount of carbon species deposited on the iron (carbide) based catalyst was −2.5-fold higher at 300 °C than at 250 °C. TGA analysis suggests that the laydown on the iron (carbide) catalyst mostly consists of heavy hydrocarbon products (and not polyaromatic coke species).

In contrast operating the zeolite at 300 °C led to only −25-50 % of the carbon deposit compared to experiments performed at 250 °C. At 250 °C, mainly condensed heavy hydrocarbons were detected (decomposing in the TGA between 200 °C and 400 °C). After operation at 275 − 300 °C, instead coke species decomposing in the TGA at higher temperature (450 − 650 °C) were found. This shows that at 250 °C heavy hydrocarbons formed on the iron (carbide) catalyst condense in the pores of the zeolite without being converted, while at higher temperatures they are converted (i.e. by aromatization and cracking), but coke species are formed as a consecutive product of olefin aromatization. Indeed, at 300 °C, the amount of coke formed on the zeolite increased with increasing selectivity to aromatics. A detailed TGA study can be found in the supporting information (Fig. S10-S12 and Table S1).

4. Conclusion

In this work we studied the influence of reaction conditions on the conversion of synthesis gas to aromatics with olefin intermediates by combining a potassium promoted bulk iron-based Fischer-Tropsch catalyst with an H-ZSM-5 zeolite in stacked bed mode in a single reactor. We focused on the formation of olefin intermediates with a chain length in the range of C_6-C_{10} and therefore suitable for formation of aromatics, rendering the need for oligomerization of short olefins unnecessary.

By operating the Fischer-Tropsch catalyst between 250 °C and 300 °C and 20 bar, we achieved α-values of the Anderson-Schulz-Flory distribution between 0.70 and 0.72, which predicts a high fraction of C_6-C_{10} products. Furthermore, the methane selectivity was as low as 7–14 $\%_C$.

Placing a bed of H-ZSM-5 downstream of the iron catalyst and operating at 250 °C resulted in C_6-C_{10} aromatics being formed with only 2–3 $\%_C$ selectivity. TGA measurements of the spent zeolite revealed that heavy hydrocarbon products condensed in the zeolite, indicating that reaction temperature of 250 °C is insufficient to effectively convert olefins into aromatics. Increasing the reaction temperature to 300 °C, up to 18 $\%_C$ C_6-C_{10} aromatics were formed, whereas the enhanced formation of aromatics also caused the formation of coke species in the zeolite bed.

To study the contribution of olefins with various chain length on the formation of aromatics the amount of zeolite placed downstream of the Fischer-Tropsch catalyst was varied. It was found that olefins in the range of C_4-C_8 were exclusively converted to aromatics in the initial section of the zeolite bed, whereas C_2-C_3 olefins initially remained

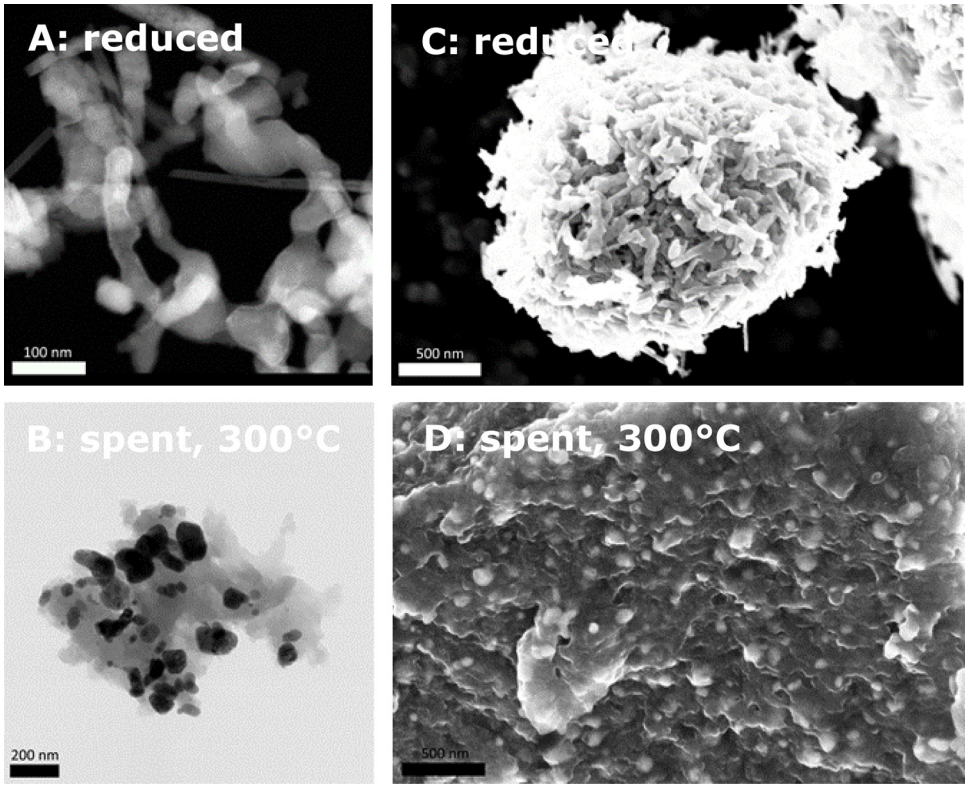

Fig. 9. High annular angle dark field scanning transmission electron microscopy (HAADF-STEM) images of **A**: reduced FeK at 350 °C for 2 h in 30 % H_2 in N_2, Bright-field TEM images of **B**: spent FeK at 300 °C and scanning electron microscopy (SEM) images of **C**: reduced FeK at 350 °C for 2 h in 30 % H_2 in N_2, **D**: spent FeK at 300 °C. Reaction conditions for spent samples: 300 °C at GHSV = 40,000 h^{-1}, 20 bar, CO:H_2 = 1 v/v, TOS = 50 h.

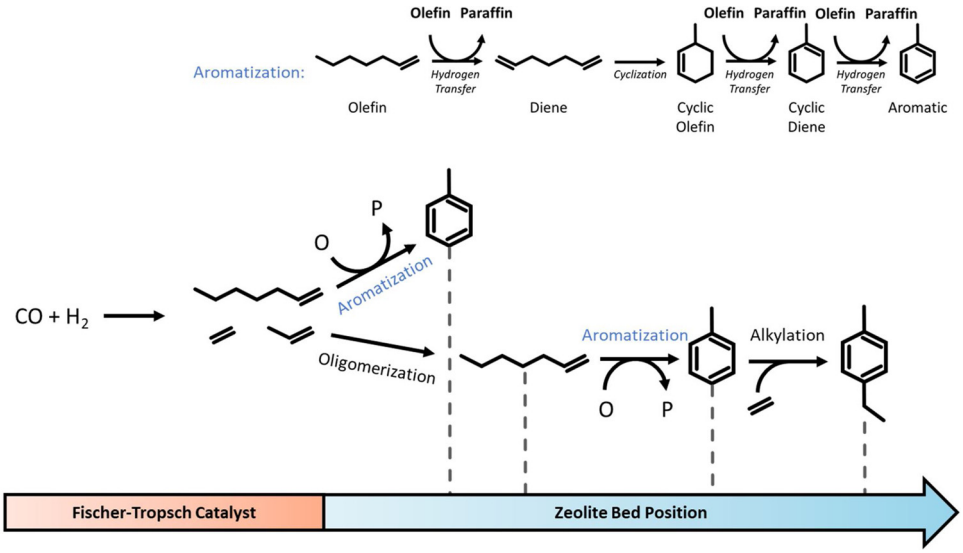

Fig. 10. Proposed pathway of formation of aromatics from synthesis gas via a mixture of long and short olefin intermediates (P denotes paraffins and O denotes olefins). The aromatization of olefin with suitable chain length is shown in detail on the top right.

untouched. In the further course of the zeolite bed, C_2-C_3 olefins underwent oligomerization, resulting in an increase in C_4-C_8 olefin selectivity, followed by further aromatization of long olefins. Furthermore, C_2-C_3 olefins contributed to alkylation of light aromatics forming ethylmethylbenzene as main product within the aromatics with a 73 $\%_C$ share in the C_9 aromatics fraction and 26 $\%_C$ in the total aromatics. The proposed pathway for the formation of aromatics from synthesis gas with short and long olefin intermediates is shown in Fig. 10.

By altering the amount of the iron catalyst loaded into the reactor while keeping the zeolite bed height downstream of the iron catalyst constant, we investigated the influence of CO conversion in a range of 3.5%–76% on the aromatization of olefin intermediates. The yield of C_6-C_{10} aromatics showed a decreasing trend with increasing CO conversion, due to a limited reactive capacity of the zeolite bed in combination with increasing yield of olefins formed on the Fischer-Tropsch catalyst.

We showed that operating a bulk iron-based Fischer-Tropsch catalyst in stacked bed with an H-ZSM-5 zeolite at appropriate reaction conditions allows to convert synthesis gas into aromatics with up to 18 $\%_C$ selectivity. However, the study of the long-term stability was not in the focus of this work and therefore, these findings can greatly contribute to set the cornerstone for the design of a process to convert synthesis gas to aromatics, whereas we unraveled the role of short and long olefins in the aromatization of Fischer-Tropsch products.

Danny Wezendonk (UU) is acknowledged for assistance with TGA-measurements. Iris ten Have (UU) and Jochem Wijten (UU) are thanked for the recording of SEM images. Savannah Turner (UU) and Nynke Krans (UU) are thanked for TEM images. Silvia Zanoni and Nikos Nikolopoulos are thanked for nitrogen and argon physisorption measurements.

Acknowledgements

This work was supported by the Netherlands Center for Multiscale Catalytic Energy Conversion (MCEC), an NWO Gravitation program funded by the Ministry of Education, Culture and Science of the government of the Netherlands. KPdJ acknowledges the European Research Council, EU FP7 ERC Advanced Grant no. 338846. This project has received funding from the European Research Council (ERC) under the European Union's Horizon 2020 research and innovation programme ERC-2014-CoG 648,991.

Appendix A. Supplementary data

Supplementary material related to this article can be found, in the online version, at doi:https://doi.org/10.1016/j.cattod.2020.05.016.

References

[1] A. Merkel, Science (80-.) 281 (1998) 336–337.
[2] R.C. Armstrong, C. Wolfram, K.P. de Jong, R. Gross, N.S. Lewis, B. Boardman, A.J. Ragauskas, K. Ehrhardt-Martinez, G. Crabtree, M.V. Ramana, Nat. Energy 1 (2016) 15020.
[3] I. Dybkjaer, Fuel Process. Technol. 42 (1995) 85–107.
[4] J.J. Hernández, G. Aranda-Almansa, A. Bula, Fuel Process. Technol. 91 (2010) 681–692.
[5] J.J. Hernández, G. Aranda-Almansa, C. Serrano, Energy Fuels 24 (2010) 2479–2488.
[6] S. Luo, L. Zeng, D. Xu, M. Kathe, E. Chung, N. Deshpande, L. Qin, A. Majumder, T.L. Hsieh, A. Tong, Z. Sun, L.S. Fan, Energy Environ. Sci. 7 (2014) 4104–4117.
[7] H.M. Torres Galvis, J.H. Bitter, C.B. Khare, M. Ruitenbeek, A.I. Dugulan, K.P. De Jong, Science (80-.) 335 (2012) 835–838.
[8] H.M. Torres Galvis, A.C.J. Koeken, J.H. Bitter, T. Davidian, M. Ruitenbeek, A.I. Dugulan, K.P. De Jong, Catal. Today 215 (2013) 95–102.
[9] J. Su, D. Wang, Y. Wang, H. Zhou, C. Liu, S. Liu, C. Wang, W. Yang, Z. Xie, M. He, ChemCatChem 10 (2018) 1536–1541.
[10] F. Jiao, J. Li, X. Pan, J. Xiao, H. Li, H. Ma, M. Wei, Y. Pan, Z. Zhou, M. Li, S. Miao, J. Li, Y. Zhu, D. Xiao, T. He, J. Yang, F. Qi, Q. Fu, X. Bao, Science (80-.) 351 (2016) 1065–1068.
[11] S.M.G. Lama, J.L. Weber, T. Heil, J.P. Hofmann, R. Yan, K.P. de Jong, M. Oschatz, Appl. Catal. A Gen. 568 (2018) 213–220.
[12] M. Oschatz, W.S. Lamme, J. Xie, A.I. Dugulan, K.P. de Jong, ChemCatChem 8 (2016) 2846–2852.
[13] H. Schulz, M. Claeys, Appl. Catal. A Gen. 186 (1999) 91–107.
[14] M. Oschatz, N. Krans, J. Xie, K.P. de Jong, J. Energy Chem. 25 (2016) 985–993.
[15] M. Casavola, J. Xie, J.D. Meeldijk, N.A. Krans, A. Goryachev, J.P. Hofmann, A.I. Dugulan, K.P. De Jong, ACS Catal. 7 (2017) 5121–5128.
[16] N.A. Krans, E.C. van der Feltz, J. Xie, A.I. Dugulan, J. Zečević, K.P. de Jong, ChemCatChem 10 (2018) 3388–3391.
[17] K. Cheng, W. Zhou, J. Kang, S. He, S. Shi, Q. Zhang, Y. Pan, W. Wen, Y. Wang, Chem 3 (2017) 334–347.
[18] W. Zhou, J. Kang, K. Cheng, S. He, J. Shi, C. Zhou, Q. Zhang, J. Chen, L. Peng, M. Chen, Y. Wang, Angew. Chemie Internatioanl Ed. 130 (2018) 12188–12192.
[19] F. Jiao, X. Pan, K. Gong, Y. Chen, G. Li, X. Bao, Angew. Chemie Int. Ed. 57 (2018) 4692–4696.
[20] Y. Zhu, X. Pan, F. Jiao, J. Li, J. Yang, M. Ding, Y. Han, Z. Liu, X. Bao, ACS Catal. 7 (2017) 2800–2804.
[21] H. Xu, Z. Huang, S. Wang, F. Qin, L. Huang, Y. Yue, W. Hua, H. He, W. Shen, ChemCatChem (2018), https://doi.org/10.1002/cctc.201800911.
[22] T. Yang, L. Cheng, N. Li, D. Liu, Ind. Eng. Chem. Res. 56 (2017) 11763–11772.
[23] W. Zhou, S. Shi, Y. Wang, L. Zhang, Y. Wang, G. Zhang, X. Min, K. Cheng, Q. Zhang, J. Kang, Y. Wang, ChemCatChem (2019), https://doi.org/10.1002/cctc.201801937.
[24] C. Beasley, M.K. Gnanamani, H.H. Hamdeh, M. Martinelli, B.H. Davis, Catal. Letters 148 (2018) 1920–1928.

[25] A.V. Karre, A. Kababji, E.L. Kugler, D.B. Dadyburjor, Catal. Today 214 (2013) 82–89.
[26] A.V. Karre, A. Kababji, E.L. Kugler, D.B. Dadyburjor, Catal. Today 198 (2012) 280–288.
[27] Y. Xu, J. Liu, G. Ma, J. Wang, Q. Wang, J. Lin, H. Wang, C. Zhang, M. Ding, Mol. Catal. 454 (2018) 104–113.
[28] Q. Yan, Y. Lu, C. Wan, J. Han, J. Rodriguez, J.J. Yin, F. Yu, Energy Fuels 28 (2014) 2027–2034.
[29] Y. Xu, J. Liu, G. Ma, J. Wang, J. Lin, H. Wang, Fuel 228 (2018) 1–9.
[30] B. Zhao, P. Zhai, P. Wang, J. Li, T. Li, M. Peng, M. Zhao, G. Hu, Y. Yang, Y.W. Li, Q. Zhang, W. Fan, D. Ma, Chem 3 (2017) 323–333.
[31] N. Guan, Y. Liu, M. Zhang, Catal. Today 30 (1996) 207–213.
[32] J.L. Weber, I. Dugulan, P.E. de Jongh, K.P. de Jong, ChemCatChem 10 (2018) 1107–1112.
[33] J.L. Weber, N.A. Krans, J.P. Hofmann, E.J.M. Hensen, J. Zecevic, P.E. de Jongh, K.P. de Jong, Catal. Today (2019), https://doi.org/10.1016/j.cattod.2019.02.002.
[34] X.Y. Gwagwa, E. van Steen, Chem. Eng. Technol. 32 (2009) 826–829.
[35] F.G. Botes, W. Böhringer, Appl. Catal. A Gen. 267 (2004) 217–225.
[36] F.G. Botes, Appl. Catal. A Gen. 284 (2005) 21–29.
[37] A. Nakhaei Pour, S.M.K. Shahri, Y. Zamani, M. Irani, S. Tehrani, J. Nat. Gas Chem. 17 (2008) 242–248.
[38] M.E. Dry, Catal. Today 71 (2002) 227–241.
[39] D. Walter, G. Buxbaum, W. Laqua, J. Therm, Anal. Calorim. 63 (2001) 733–748.
[40] D.J. Moodley, J. van de Loosdrecht, A.M. Saib, M.J. Overett, A.K. Datye, J.W. Niemantsverdriet, Appl. Catal. A Gen. 354 (2009) 102–110.
[41] V. Gruver, R. Young, J. Engman, H.J. Robota, Prepr. - Am. Chem. Soc. Div. Pet. Chem. (2005) 164–166.
[42] M.E. Dry, J. Chem. Technol. Biotechnol. 77 (2002) 43–50.
[43] S. Müller, Y. Liu, F.M. Kirchberger, M. Tonigold, M. Sanchez-Sanchez, J.A. Lercher, J. Am. Chem. Soc. 138 (2016) 15994–16003.
[44] G. Giannetto, A. Montes, N.S. Gnep, A. Florentino, P. Cartraud, M. Guisnet, J. Catal. 145 (1994) 86–95.